Collectivity of dipole bands in ^{196}Pb

E. F. Moore,[1] M. P. Carpenter,[2] Y. Liang,[2,*] R. V. F. Janssens,[2] I. Ahmad,[2] I. G. Bearden,[2,3] P. J. Daly,[3] M. W. Drigert,[4] B. Fornal,[3] U. Garg,[5] Z. W. Grabowski,[3] H. L. Harrington,[1] R. G. Henry,[2] T. L. Khoo,[2] T. Lauritsen,[2] R. H. Mayer,[3] D. Nisius,[3] W. Reviol,[5,†] and M. Sferrazza[3]

[1]*North Carolina State University, Raleigh, North Carolina 27695 and Triangle Universities Nuclear Laboratory, Durham, North Carolina 27708*

[2]*Argonne National Laboratory, Argonne, Illinois 60439*

[3]*Purdue University, West Lafayette, Indiana 47907*

[4]*Idaho National Engineering Laboratory, EG&G Idaho Inc., Idaho Falls, Idaho 83415*

[5]*University of Notre Dame, Notre Dame, Indiana 46556*

(Received 9 September 1994)

The lifetimes of states in two of the $\Delta I = 1$ bands in ^{196}Pb have been measured using the Doppler shift attenuation method, and a new $\Delta I = 1$ band has been observed in this nucleus. States in the bands were populated in the reaction ^{170}Er(^{30}Si,4n) at a beam energy of 142 MeV. Individual level lifetimes were extracted from the data by an analysis of the Doppler broadened γ-ray line shapes. Under the assumption of pure $M1$ radiation, average reduced transition strengths $B(M1) \sim 1.5$ W.u. were obtained. The $B(M1)$ values in both the "regular" and "irregular" bands exhibit similar dependence on spin. The neutron and proton configurations and nature of the collectivity in these bands is discussed.

PACS number(s): 21.10.Re, 21.10.Tg, 21.60.Ev, 27.80.+w

I. INTRODUCTION

The region of nuclei with mass $A \sim 190$ has been studied extensively over the last few years following the discovery of superdeformation in ^{191}Hg [1]. The status of superdeformation studies in this region is reviewed in Ref. [2]. More recently, considerable interest in the neutron-deficient Pb isotopes has developed with the discovery of a number of bands at high spin connected by dipole transitions in both even $^{192-200}$Pb [3–12] and odd $^{197-201}$Pb [13–15] nuclei. In contrast with the single-particle nature of the low-spin excitations in these semimagic nuclei, the dipole bands exhibit enhanced $M1$ transition strength. The majority of the dipole bands in the Pb nuclei are "regular" in character (i.e., transition energies increase smoothly with spin). The regular bands are characterized by large $B(M1)/B(E2)$ ratios and dynamic moments of inertia $\mathcal{J}^{(2)}$ significantly smaller than the kinematic moments of inertia $\mathcal{J}^{(1)}$, indicative of large amounts of aligned angular momentum. In addition, sequences of dipole transitions exhibiting "irregular" transition energy characteristics have also been observed in many of the same nuclei. The properties of the dipole bands have been interpreted in terms of high-K, moderately deformed oblate states built on configurations involving high-j, shape driving quasiproton excitations coupled to rotation-aligned quasineutrons.

In the case of ^{196}Pb, two regular bands and one irregular band have recently been identified [6]. It is of interest to note that the irregular band was populated more strongly than the regular bands. For one of the regular bands in this nucleus (band 2 in the notation of Ref. [6]), the transitions linking it to the known yrast levels were observed, allowing the experimental determination of the spins and excitation energies of states within the band. A configuration of $\pi(h_{9/2} \otimes i_{13/2}) \otimes \nu(i_{13/2})^2$ was assigned [6] to this band. On the other hand, the configuration associated with the irregular band in this nucleus is not well understood. Various mechanisms leading to a strong irregular band were explored, but the experimental data did not allow for a definite configuration assignment [6].

Important information concerning the degree of collectivity of these bands can be provided by lifetime measurements. In addition, lifetime measurements also provide a means of testing proposed single-particle configurations. Recent Doppler shift attenuation method (DSAM) and recoil distance method (RDM) lifetime measurements in ^{197}Pb [16,17] and ^{198}Pb [9,17] have found significant dipole strength, $B(M1) \sim 1$–2 Weisskopf units (W.u.) associated with regular bands in these nuclei, while the observed in-band $B(E2)$ values suggest only modest ($\beta_2 \sim 0.1$) quadrupole deformation. In contrast, the $B(M1)$ and $B(E2)$ values derived from RDM lifetime measurements in the irregular band of ^{197}Pb [17] indicate a significant reduction in both dipole strength and quadrupole collectivity when compared to the regular bands. Taken in combination with the pronounced differences in the behavior of the transition energies, this observation supports the interpretation that the irregular bands are based on very different configurations from those associated with the regular bands. The presence of

*Present address: Dept. of Radiology, Indiana University Medical Center, Indianapolis, IN 46202.

†Present address: Physics Dept., University of Tennessee, Knoxville, TN 37996.

both regular and irregular dipole bands in the neighboring nucleus ^{196}Pb provides an excellent opportunity to test whether these characteristics are common to dipole bands in other nuclei of the region. We report on spectroscopic and lifetime measurements carried out for regular and irregular bands in the nucleus ^{196}Pb.

II. EXPERIMENT AND RESULTS

A. Level scheme

Excited states in ^{196}Pb were populated using the reaction ^{170}Er(^{30}Si, $4n$). Two experiments were performed. The first measurement used a target consisting of two 500 μg/cm^2 ^{170}Er self-supporting foils isotopically enriched to 95%. Beam energies of 142, 146, and 151 MeV were supplied by the ATLAS accelerator facility at Argonne National Laboratory. The γ rays were detected in the Argonne-Notre Dame BGO γ-ray facility, which consists of 12 Compton suppressed Ge spectrometers (CSG's) surrounding an inner array of 50 hexagonal bismuth Germanate (BGO) elements. The CSG's are positioned at angles of 34.5°, 90°, and 145.5° to the beam direction, with four detectors at each angle. A threshold of two or more CSG's and a minimum of 3 BGO elements firing in prompt coincidence were required for the events to be recorded. The energy and timing information from the CSG's and the fold and sum energy derived from the array were written on tape. Further experimental details may be found in Ref. [18]. Approximately 3×10^8 γ-γ coincidence events were accumulated during the three thin-target measurements. By placing appropriate gates on the array multiplicity distributions, coincidence matrices were produced with the relative ^{196}Pb content enhanced to about 80% at each beam energy.

All transitions assigned to bands 1–3 in Ref. [6] have been observed in the present work and their placement is consistent with the proposed level scheme. The transition energies, intensities, and directional correlation (DCO) ratios of bands 1–3 are summarized in Tables I–III, respectively. The analysis of our data also revealed a fourth band in ^{196}Pb with characteristics similar to those of the other regular dipole bands in this nucleus, but with weaker intensity. Stretched $\Delta I = 1$ multipolarity was determined from the measured directional correlations.

TABLE I. Energies, relative intensities, and directional correlation (DCO) ratios for transitions assigned to band 1 in ^{196}Pb. The transition intensities were obtained from a combination of singles and coincidence data and are normalized to the 958.6 keV transition, the intensity of which is taken to be 100.

E_γ (keV)	Relative intensity	DCO ratio
164.4	9.7(9)	0.58(8)
208.5	10.3(7)	0.61(8)
249.9	9.3(6)	0.68(10)
309.1	9.4(6)	0.71(8)
375.8	5.7(4)	0.78(10)
404.5	3.9(5)	0.65(8)

TABLE II. Energies, relative intensities, directional correlation (DCO) ratios, and spin assignments for transitions assigned to band 2 and the corresponding transitions which link band 2 to the lower spin states in ^{196}Pb. The transition intensities were obtained from a combination of singles and coincidence data and are normalized to the 958.6 keV transition, the intensity of which is taken to be 100.

E_γ (keV)	Relative intensity	DCO ratio	Assignment
107.6	~ 28		$17^{(-)} \rightarrow 16^{(-)}$
137.6	27.7(19)	0.72(20)	$18^{(-)} \rightarrow 17^{(-)}$
204.1	22.2(9)	0.54(10)	$19^{(-)} \rightarrow 18^{(-)}$
268.4	17.6(6)	0.62(7)	$20^{(-)} \rightarrow 19^{(-)}$
332.4	15.3(5)	0.53(6)	$21^{(-)} \rightarrow 20^{(-)}$
342	< 2		$19^- \rightarrow 17^-$
367.2	12.4(6)	0.65(8)	$22^{(-)} \rightarrow 21^{(-)}$
392.1	10.3(6)	0.59(9)	$23^{(-)} \rightarrow 22^{(-)}$
397.9	6.2(4)	0.61(7)	$24^{(-)} \rightarrow 23^{(-)}$
408.4	5.9(4)	0.75(9)	$25^{(-)} \rightarrow 24^{(-)}$
422.1	3.7(3)	0.70(10)	$26^{(-)} \rightarrow 25^{(-)}$
428.8	2.0(3)		$27^{(-)} \rightarrow 26^{(-)}$
472	< 2		$20^- \rightarrow 18^-$
309.0	9.4(5)	0.63(10)	$13^- \rightarrow 12^-$
502.1	17.6(2)	0.51(7)	$16^{(-)} \rightarrow 15^-$
546.4	9.4(5)	0.47(9)	$12^- \rightarrow 11^-$
605.5	18.0(2)	1.05(9)	$15^- \rightarrow 13^-$
855.2	8.6(4)	1.12(15)	$13^- \rightarrow 11^-$

Table IV presents the energies, relative intensities, and DCO results for the transitions assigned to this band. Coincidence spectra gated on transitions in bands 1–4 are presented in Figs. 1(a)–(d), respectively. The relevant level scheme of ^{196}Pb is shown in Fig. 2.

The γ-ray energies in band 4 exhibit a regular increase with increasing spin, consistent with a rotational nature. Transitions in the lower-lying level scheme of ^{196}Pb were observed to be in coincidence with gates on members of

TABLE III. Energies, relative intensities, and directional correlation (DCO) ratios for transitions assigned to band 3 in ^{196}Pb. The transition intensities were obtained from a combination of singles and coincidence data and are normalized to the 958.6 keV transition, the intensity of which is taken to be 100.

E_γ (keV)	Relative intensity	DCO ratio
192.6	36.6(6)	0.46(6)
314.7	37.0(6)	0.54(6)
374.6	23.3(7)	0.54(4)
355.5	20.1(6)	0.62(6)
341.8	20.4(5)	0.65(5)
243.6	21.2(6)	0.54(5)
209.8	19.1(7)	0.44(4)
239.5	17.5(6)	0.61(6)
339.1	15.5(8)	0.60(6)
286.5	13.4(19)	0.55(6)
398.4	8.4(3)	0.56(6)
448.6	4.2(4)	0.74(13)
490.4	4.3(6)	
696.9	4.2(4)	1.10(11)
729.8	4.8(5)	1.16(8)

TABLE IV. Energies, relative intensities, and directional correlation (DCO) ratios for transitions assigned to band 4 in ^{196}Pb. The transition intensities were obtained from a combination of singles and coincidence data and are normalized to the 958.6 keV transition, the intensity of which is taken to be 100.

E_γ (keV)	Relative intensity	DCO ratio
295.7	4(1)	0.45(2)
342.8	4(1)	0.72(7)
379.9	3(1)	0.61(5)
412.7	< 2	0.47(5)
432.4	< 2	

this band, however, the data did not allow the delineation of the linking transitions. Therefore, it was not possible to assign spin and excitation energy to this band. It is worth noting that a level scheme was also obtained for ^{195}Pb from these studies, and several dipole bands were observed in this nucleus [19].

B. DSAM measurement

In the DSAM measurement, the target consisted of 1.0 mg/cm^2 of ^{170}Er evaporated on a 24 mg/cm^2 thick lead backing, and a beam energy of 142 MeV was chosen. From an initial recoil velocity of $v = 0.015c$, the recoiling Pb nuclei were slowed down in the target and backing before coming to complete rest in the backing. A total of 72 million coincidence events were stored and analyzed. In the off-line analysis, γ-γ coincidence matrices were created for all CSG angle combinations. In order to enhance the relative intensity of the $4n$ channel in the matrices, the condition of array fold ≥ 9 was required during the sorting process. The total number of coincident events satisfying this condition amounted to $\sim$ 30 million.

The coincidence spectra used in the line shape analysis were produced from the angle-sorted matrices by gating on the low-lying transitions in each band which are emitted after the residual nuclei have stopped in the Pb backing. Gated spectra were obtained for each set of detectors located at forward, backward, and 90° angles to the beam direction. The experimental Doppler broadened line shapes were compared to those calculated with the computer code LILIFI [20]. The electronic and nuclear components of the stopping power were calculated with the code TRIM85 [21]. The slowing down histories of 10^4 recoiling Pb ions in both the target and backing were traced in a Monte Carlo simulation. The effects of lateral and longitudinal straggling were included, as were corrections for the finite solid angle of the Ge detectors and the positional dependence of their efficiencies.

The line shape calculations include (i) the decay within the bands (using measured γ-ray energies and intensities); (ii) a set of precursor transitions (with the same moment of inertia) preceeding the highest known transition in each band; and (iii) side feeding into each state, approximated by a single rotational cascade of five transitions. The side-feeder bands were assumed to have a moment of inertia similar to that in the main cascade [22]. The intensites of the side-feeding cascades were constrained by the measured intensities of the in-band transitions feeding or deexciting the levels of interest. The spectra measured at forward, transverse, and backward angles were fit simultaneously. Line shape fits were

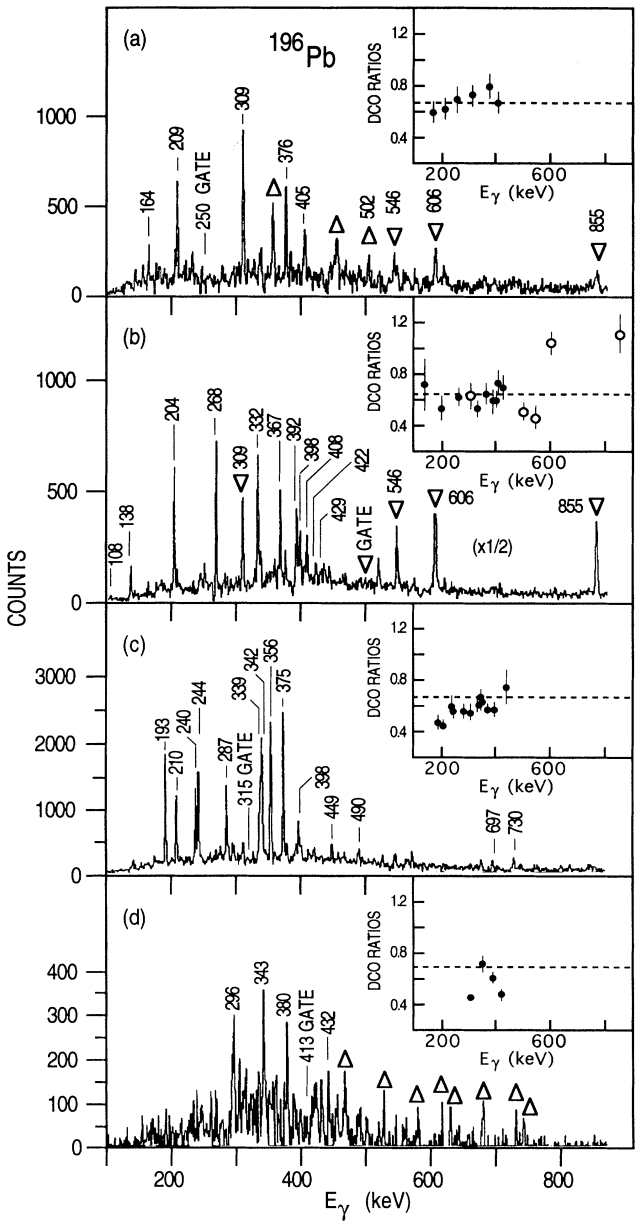

FIG. 1. Coincidence spectra gated by transitions in (a) band 1, (b) band 2, (c) band 3, and (d) band 4. The inverted triangles denote transitions belonging to the low spin part of the ^{196}Pb level scheme; the upright triangles indicate contaminant transitions which occur when one of the gating transitions is an unresolved doublet with a γ ray from another nucleus (in most cases ^{195}Pb). The experimentally measured DCO ratios are presented in the insets; the solid circles correspond to transitions within the bands and the open circles denote transitions with known multipolarity in the level scheme of ^{196}Pb.

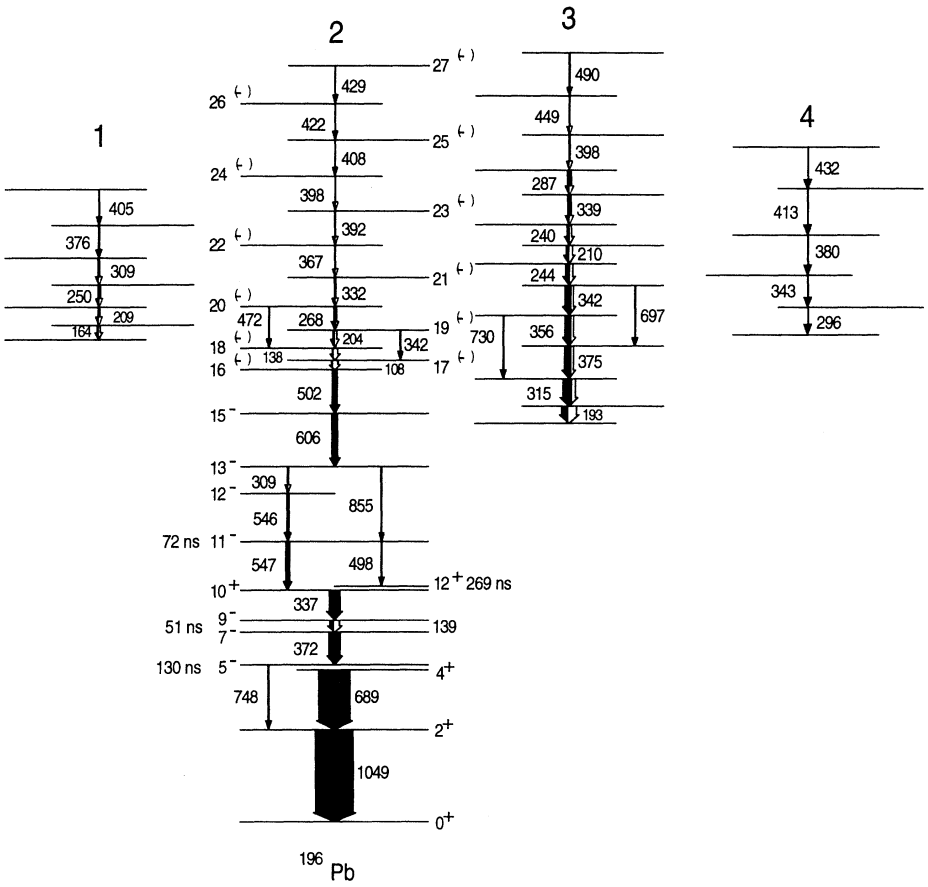

FIG. 2. Partial level scheme for ^{196}Pb showing the previously observed [6] dipole bands (bands 1–3). The newly observed band is labeled band 4. Lifetimes were measured for states in the regular and irregular bands, labeled 2 and 3, respectively.

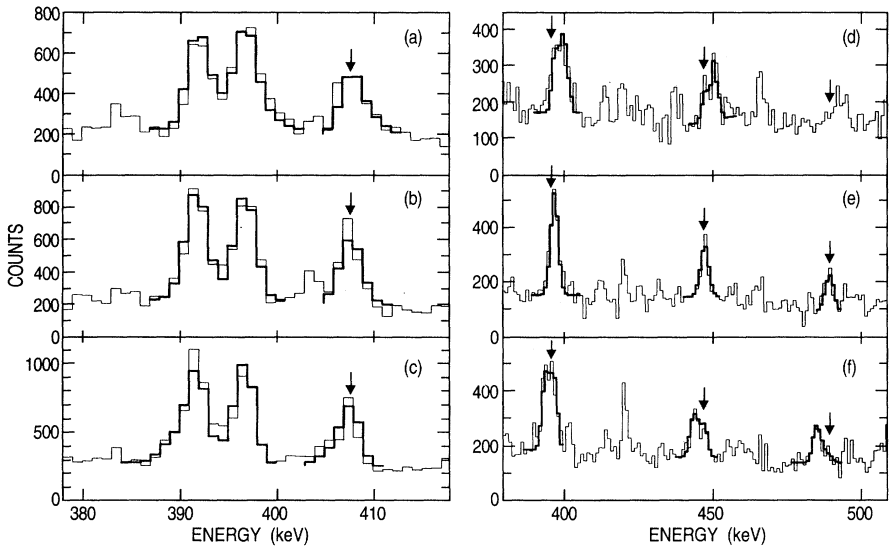

FIG. 3. Line shape fits to selected transitions in ^{196}Pb. The data are represented by thin lines. (a)–(c) show fits to the 392, 398, and 408 keV transitions in band 2, as measured in detectors at: (a) forward, (b) transverse, and (c) backward angles. (d)–(f) present fits to the 398, 449, and 490 keV transitions in band 3 at (d) forward, (e) transverse, and (f) backward angles. The spectra were constructed from the sum of several coincidence gates as described in the text. The arrows mark the positions of the unshifted γ-ray energies. Note that while the 490 keV transition clearly exhibits a large Doppler shift, the presence of a strong contaminant line prevented a reliable line shape fit to the forward angle spectrum (d).

performed on individual transitions and global fits to all transitions in each band were carried out as well. The global fits allow for correlations between the variable fit parameters of each state.

As illustrated in Fig. 3, the measured line shapes are well reproduced in the fitting process. The mean lifetimes extracted from the fits are listed in Table V. The quoted errors include statistical uncertainties as well as uncertainties due to the treatment of side-feeding lifetimes and intensities. Not included in the errors is the uncertainty in the slowing down process associated with the stopping power calculation. While this uncertainty may be as large as 20%, it does not alter the results when comparing the relative dipole strength between the two bands.

After correction for internal conversion, the $B(M1)$ values were derived from the measured lifetimes under the assumption of pure $M1$ character. The $B(M1)$ values extracted from the present data (see Table V) are comparable to those obtained in similar studies in ^{197,198}Pb [16,9,17], i.e., $B(M1) \sim 1.5$ W.u. Since $E2$ branches were not observed for those states with measurable lifetimes, it is not possible to extract $B(E2)$ values for the bands in ^{196}Pb. However, due to the absence of $E2$ branches, one may conclude that the magnitude of $E2$ collectivity in these bands is comparable to or smaller than that in ^{197,198}Pb. For example, our experimental sensitivity is such that a 10% $E2$ branch in the irregular band should be observable; if one assumes a 10% $E2$ branching ratio limit for the 398 + 287 keV transitions and uses the measured lifetime of 0.25 ps, one obtains an upper limit of $B(E2) < 32$ W.u. This limit is comparable to the $B(E2)$ values measured [16,9,17] in ^{197,198}Pb.

TABLE V. Summary of lifetime results for dipole bands in ^{196}Pb. The state lifetimes along with the energies of the deexciting γ rays are given. The reduced transition probabilities $B(M1)$ are presented (W.u. stands for Weisskopf unit), under the assumption that the transitions are of a pure $M1$ character.

Band	E_γ (keV)	τ (ps)	$B(M1)$ (μ_N^2)	$B(M1)$ (W.u.)
2	367.2	≤ 0.4	≥ 2.3	≥ 1.3
	392.1	$0.21(^{+15}_{-12})$	$3.7(^{+49}_{-16})$	$2.1(^{+28}_{-9})$
	397.9	$0.17(^{+12}_{-8})$	$4.4(^{+39}_{-18})$	$2.5(^{+22}_{-10})$
	408.4	0.39(11)	$1.8(^{+7}_{-4})$	$1.0(^{+4}_{-2})$
	422.1	$0.47(^{+10}_{-14})$	$1.4(^{+6}_{-2})$	$0.8(^{+3}_{-1})$
	428.8	0.23(9)	$2.7(^{+17}_{-8})$	$1.5(^{+10}_{-4})$
3	339.1	$0.35(^{+20}_{-10})$	$3.2(^{+13}_{-12})$	1.8(7)
	286.5	0.41(8)	$3.9(^{+10}_{-6})$	$2.2(^{+5}_{-4})$
	398.4	0.25(6)	$3.0(^{+10}_{-6})$	$1.7(^{+5}_{-3})$
	448.6	0.27(4)	$2.0(^{+4}_{-3})$	1.1(2)
	490.4	0.23(5)	$1.9(^{+5}_{-3})$	$1.1(^{+3}_{-2})$

III. DISCUSSION

A. Structure of the $\Delta I = 1$ bands

A large number of $\Delta I = 1$ bands are now known in Pb isotopes and it is generally accepted that these sequences are built upon weakly deformed high-K quasiproton configurations coupled to rotation-aligned high-j quasineutrons. Configuration-constrained shell model calculations [23] have shown that the $K^\pi = 11^-$ isomeric level observed in ^{194,196}Pb [24,25] is based on the $\pi(h_{9/2} \otimes i_{13/2})$ two-quasiproton configuration, consistent with the measured g factors [25]. The calculations indicate that the deformation corresponding to this configuration is $\beta_2 \sim -0.15$. Thus it is expected that rotational bands built on this configuration should exist. Other low-lying high-K quasiproton configurations at small oblate deformations ($\beta_2 \sim -0.1$) in the Pb isotopes are the $\pi(h_{9/2})^2_{K=8}$ and $\pi(h_{9/2} \otimes s_{1/2})_{K=5}$ structures (see, for example, Fig. 13 of Ref. [10]) and rotational bands based on these configurations are possible as well.

For small oblate deformation, the neutron shell structure near $N = 114$ is determined by the $i_{13/2}$, $p_{3/2}$, and $f_{5/2}$ single-particle orbitals; in cranking notation (with pairing) the $i_{13/2}$ neutron orbitals are labeled A, B, C, and D, whereas the lowest-lying negative parity Routhians associated with the $f_{5/2}$ and $p_{3/2}$ orbitals are denoted by E and F, respectively. The positive parity neutron orbitals consist of the low-Ω members of the $i_{13/2}$ spherical state, which carry large amounts of aligned angular momentum; a feature observed in the $\Delta I = 1$ bands. The structure of the $M1$ bands have been interpreted within the framework of one- and three-dimensional cranking calculations, both as paired and unpaired bands. The properties of the bands in ^{196}Pb will be compared to those of $M1$ bands in other Pb isotopes and discussed in terms of the cranked shell model calculations of Refs. [6,10].

1. Regular bands

The moments of inertia for the regular dipole bands (bands 1, 2, and 4) in ^{196}Pb are plotted in Fig. 4. The dynamic moments of inertia ($\mathcal{J}^{(2)} = dI/d\omega = 1/\Delta E_\gamma$) were extracted from the γ-ray energies, whereas the kinematic moments of inertia ($\mathcal{J}^{(1)} = I/\omega = I/E_\gamma$) were extracted from the γ-ray energies and known spins for band 2, and were calculated for bands 1 and 4 under the assumption of bandhead spins of $17\hbar$ and $18\hbar$, respectively. The experimental uncertainties on these spin estimates are of the order of 2–$4\hbar$.

As pointed out above, the fact that the $\mathcal{J}^{(2)}$ values are considerably smaller than those for $\mathcal{J}^{(1)}$ is indicative of large amounts of aligned angular momentum. A further indication of large alignment is given in Fig. 5, where the component of the angular momentum along the rotational axis (I_x) is plotted under the assumption of $K^\pi = 11^-$. In particular, the extrapolation to $\hbar\omega = 0$ gives an initial alignment of ~ 10–$11\hbar$ for band 2. Since the bandhead spins have not been experimentally established

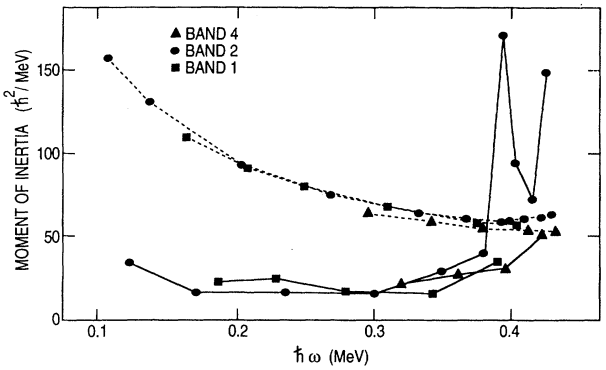

FIG. 4. Moments of inertia vs rotational frequency for the regular bands in ^{196}Pb. The dynamic moment of inertia ($\mathcal{J}^{(2)} = 1/\Delta E_\gamma$) is denoted by the solid lines; the dashed lines represent the kinematic moment of inertia ($\mathcal{J}^{(1)} = I/E_\gamma$). The kinematic moments were derived under the assumption of bandhead spins of 17 and 18 $\hbar$ for bands 1 and 4, respectively (see text for details).

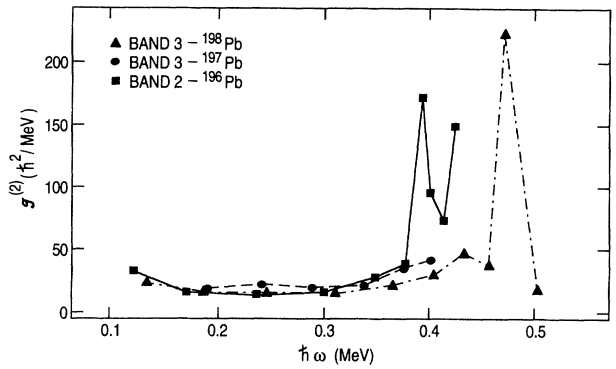

FIG. 6. Comparison of $\mathcal{J}^{(2)}$ curves for band 2 in ^{196}Pb, band 3 in ^{197}Pb (in the notation of Ref. [13]), and band 3 of ^{198}Pb (in the notation of Ref. [10]).

for bands 1 and 4, it is difficult to draw conclusions as to the degree of their initial alignment. However, the similarities of their $\mathcal{J}^{(2)}$ behaviors when compared to band 2 (see Fig. 4) suggest similar properties.

It is instructive to compare band 2 in ^{196}Pb to bands in neighboring Pb isotopes. Figure 6 shows that the behavior of $\mathcal{J}^{(2)}$ vs $\hbar\omega$ for band 2 is very similar to that of band 3 in ^{198}Pb [10] and band 3 in ^{197}Pb [13] (following the notation of the original references), especially at low frequencies. All three bands have $\mathcal{J}^{(2)}$ values of $\sim 20\ \hbar^2$/MeV over the frequency range $0.15 \leq \hbar\omega \leq 0.30$ MeV and exhibit a gradual rise in the range $0.30 \leq \hbar\omega \leq 0.40$ MeV. A dramatic rise in $\mathcal{J}^{(2)}$ occurs at $\hbar\omega \sim 0.38$ MeV in band 2 of ^{196}Pb, whereas a comparable large rise in $\mathcal{J}^{(2)}$ for band 3 in ^{198}Pb occurs at significantly higher rotational frequency, $\hbar\omega \sim 0.45$ MeV.

As was noted in Ref. [6], most of the flux from the decay out of band 2 of ^{196}Pb proceeds through the 11^- state at 3.195 MeV [i.e., the $\pi(h_{9/2} \otimes i_{13/2})$ structure]. From the cranked shell model (CSM) calculations of Ref. [6], band 2 was interpreted as the same $(h_{9/2} \otimes i_{13/2})$ proton configuration coupled to $\nu(i_{13/2})^2$. The upbend in $\mathcal{J}^{(2)}$ at $\hbar\omega \sim 0.38$ MeV could then be attributed [6] to the alignment of a second pair of $i_{13/2}$ quasineutrons (i.e., the so-called CD crossing). The absence of a sharp rise in the otherwise very similar $\mathcal{J}^{(2)}$ curve for band 3 of ^{197}Pb may indicate that either this alignment is blocked by the occupation of an $i_{13/2}$ quasineutron in the C orbital, or is delayed beyond the experimentally measured frequencies (see Fig. 6). In the case of band 3 in ^{198}Pb, it is thought that pairing is very weak and that the band can be treated as an unpaired structure [10]. In contrast, the interpretation of the upbend in terms of a CD crossing implies that these bands initially have some degree of pairing prior to the alignment and that the alignment in ^{198}Pb is delayed to higher frequency.

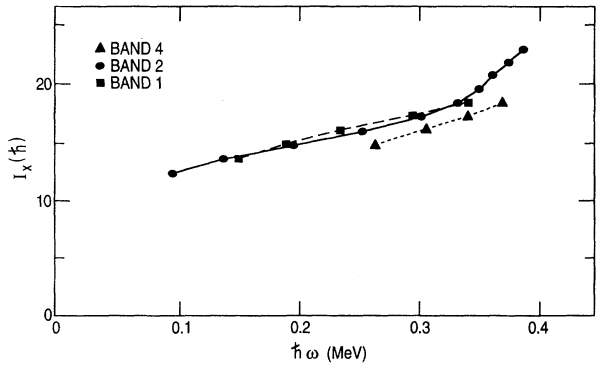

FIG. 5. Component of the angular momentum along the rotation axis as a function of rotational frequency for the regular bands in ^{196}Pb (see text for details).

As an alternative, one may interpret band 2 in ^{196}Pb as an unpaired structure, as suggested in [10]. The yrast $M1$ band in ^{196}Pb is predicted to have a $\nu 6^{-4}5^{-2}$ configuration [10] (i.e., four neutron holes in the $N = 6$ orbitals and two in the $N = 5$ orbitals relative to neutron number 120). The observed upbend would then result from the crossing of an unoccupied $N = 5, \alpha = 1/2$ orbital with one originating from the $h_{9/2}$ subshell (see, for example, Fig. 11 of Ref. [10]). This interpretation then puts band 2 of ^{196}Pb on the same footing as band 3 in ^{198}Pb. It is worth noting that the crossing occurs at lower frequency in ^{196}Pb.

The single-particle interpretation is also consistent with the observation, in both ^{198}Pb and ^{200}Pb, of $M1$ bands with nearly constant $\mathcal{J}^{(2)}$ values over the measured frequency range. This structure has been interpreted [10] as $\nu(i_{13/2})^{-4}$ in ^{198}Pb, whereas a neutron configuration of $(i_{13/2})^{-2}$ was assigned [12] to the constant $\mathcal{J}^{(2)}$ band in ^{200}Pb, and for both configurations the $N = 5$ and $h_{9/2}$ orbitals are occupied, which blocks the crossing observed in band 2 in ^{196}Pb and results in the constant moment of inertia. Both of the interpretations outlined above result in a band with negative parity, consistent with observation.

It is difficult to make configuration assignments to bands 1 and 4 since neither their spins nor excitation energies have been measured. In addition, neither band

exhibits any features associated with band crossings. In the paired scenario, the bands could be based on $ABCE$ and $ABCF$ neutron excitations, similar to ^{200}Pb. However, the spins would need to be higher than suggested by the decay patterns in order to have sufficient initial alignment. In the unpaired picture, the predicted neutron configurations would involve single-particle excitations from the occupied $h_{9/2}$ orbital to the $N = 5$ orbitals mentioned above. The lowest excitation is, in fact, the band which crosses band 2 at $\hbar\omega \sim 0.35$ MeV. The proton configurations associated with these bands could either be $(h_{9/2} \otimes i_{13/2})$ or $(h_{9/2})^2$ (i.e., high K), as suggested in Ref. [6].

2. *Irregular bands*

Dipole bands with irregular energy spacings have been observed in several Pb isotopes. Figure 7 compares the behavior of angular momentum as a function of rotational frequency for the irregular band in ^{196}Pb with those reported in ^{197,198}Pb [13,10] using the spin values proposed in the original references. The plots exhibit similar characteristics for all the bands. The irregular energy spacings have been interpreted as an indication that these bands may be based on configurations with smaller collectivity than those associated with the regular bands.

The total Routhian surface (TRS) calculations of Ref. [10] indicate that the $\pi(h_{9/2} \otimes s_{1/2})$ structures are almost spherical with $\beta_2 \sim 0.07$. The authors propose that the irregular band in ^{198}Pb (as well as the irregular band in ^{197}Pb) may be based on this weakly deformed proton configuration. The $B(E2)$ values extracted from the lifetime measurements in the irregular band of ^{197}Pb [17] are consistent with very small deformation (i.e., values of $\beta_2 \sim 0.03$ were obtained). It is also possible that configurations for which the potential energy surfaces are soft in the γ degree of freedom may be responsible for the lack of a well-defined rotational pattern in the transition energies of these bands. It was proposed [6] that in the case of ^{196}Pb, one such configuration may involve the $\pi(d_{3/2} \otimes h_{9/2})$ orbitals, based on the results of TRS calculations which indicate that this is the lowest negative parity two-quasiproton configuration at spins of $\sim 18\hbar$; a feature which could account for the observed feeding intensity. While transitions linking the irregular band to lower-lying states in ^{196}Pb have not been identified, the observation that this band is populated with greater intensity than the regular bands suggests that this sequence is based on a configuration that is lower in excitation energy (a similar conclusion was noted for the irregular band in ^{197}Pb [13]). Furthermore, the $\pi(d_{3/2} \otimes h_{9/2})$ configuration corresponds to a small oblate deformation ($\beta_2 \sim 0.1$) and is also soft in the γ direction.

It was shown in Ref. [3] that for the case of ^{192}Pb, the irregular $M1$ sequences could be subdivided into a pair of $\Delta I = 2$ bands. This approach has the advantage that effects due to signature splitting will not distort quantities of interest such as the aligned angular momentum. The two $\Delta I = 2$ sequences are then interpreted as signature partner rotational bands built on the same intrinsic configuration. We have performed this analysis on the irregular bands in ^{196,197}Pb and the resulting aligned angular momentum curves are plotted in Fig. 8. The reference parameters used in this analysis ($J_0 = 8\ \hbar$/MeV and $J_1 = 40\ \hbar^2$/MeV^2) are typical values used for oblate bands in this mass region. When the data are represented in this manner, the bands appear much less irregular than when they are treated as $\Delta I = 1$ sequences (see Fig. 7). In particular, the behavior of the alignment curves presented in Fig. 8 is consistent with the interpretation that these bands are rotational structures under-

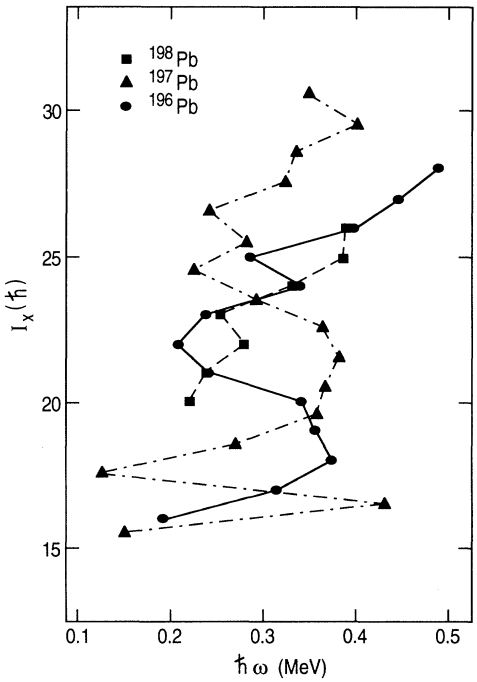

FIG. 7. Angular momentum as a function of rotational frequency for irregular bands in ^{196}Pb, ^{197}Pb [13], and ^{198}Pb [10].

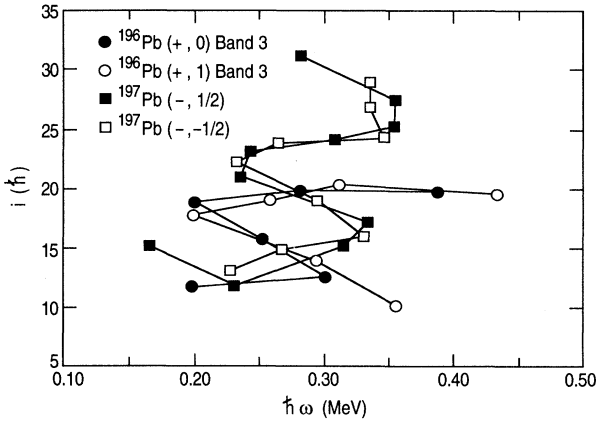

FIG. 8. Aligned angular momentum for each signature of the irregular bands in ^{196}Pb and ^{197}Pb [13]. The reference parameters used to extract the alignments are $J_0 = 8\ \hbar$/MeV and $J_1 = 40\ \hbar^2$/MeV^2. The curves are labeled by parity and signature, see text for details.

going quasiparticle alignment. The apparent irregularity of the $\Delta I = 1$ sequences then results not only from the alignments, but also from signature dependent effects.

From Fig. 8, one notes the following features: (i) a band crossing in the irregular band in ^{196}Pb occurs at $\hbar\omega = 0.25$ MeV, with a rather large gain in alignment which differs between the two signatures; (ii) the irregular band in ^{197}Pb undergoes a band crossing at $\hbar\omega = 0.28$ MeV with $\Delta i \sim 10\,\hbar$ and a second upbend occurs at a frequency of 0.35 MeV. The only quasiparticle pairs which are predicted to align at frequencies lower than 0.30 MeV are the $i_{13/2}$ neutrons. Assuming that the initial configuration for the irregular band in ^{197}Pb contains only one $i_{13/2}$ quasineutron (A), then the backbend at $\hbar\omega = 0.28$ MeV would correspond to the neutron BC crossing (in the standard cranking notation). This situation would be analogous to that of the ^{199}Pb band discussed in Refs. [12,26] using the tilted cranking model; both the crossing frequency and the alignment gain are consistent with the ^{199}Pb case. Since the feeding pattern to low-lying states observed in ^{197}Pb is indicative of large initial alignment, this suggests an AEF neutron configuration at low spin and a neutron $AEFBC$ configuration above the crossing. The presence of the EF neutrons gives the required initial alignment and also allows the BC crossing to occur. The origin of the upbend at higher frequency is not clear.

A similar situation is proposed for the irregular band in ^{196}Pb. One should note that above the backbend, the aligned angular momentum remains rather constant at $i \sim 20\hbar$ for seven transitions (see Fig. 8), indicating a rather regular behavior. Using the same arguments as for ^{197}Pb, this configuration is unlikely to have more than one $i_{13/2}$ neutron coupled to it, resulting in two possible scenarios: (i) the coupling of AE or AF neutrons to the protons at low spin with the alignment due to the BC crossing; (ii) an initial EF neutron configuration being crossed by AB $(i_{13/2})^2$ neutrons. Without knowing the initial alignment associated with this band, it is difficult to distinguish between the two possibilities.

As the above analysis shows, the irregular bands exhibit signature splitting, unlike the regular bands. Thus, the proposed $\pi(h_{9/2} \otimes s_{1/2})_{K=5}$ configuration may well be appropriate. Therefore, the irregularities observed in these bands are not necessarily directly related to the collectivity of the bands but rather associated with the configuration of the band. In recent three-dimensional (3D) cranking calculations [12], the regularity of the $M1$ sequences results in a continual reorientation of the cranking axis which is determined by the competition between the deformation aligned protons ($K = 11$) and the rotationally aligned neutrons (the so-called "shear" effect). It was shown in Ref. [12] that for structures built on the suggested proton configuration of the irregular bands, the aligned neutrons force the cranking axis to be perpendicular to the symmetry axis, where signature splitting of the bands would be expected. Indeed, one-quasiproton bands built on the $i_{13/2}$ and $h_{9/2}$ configurations observed in the Tl isotopes exhibit some signature splitting (Ref. [3]). The fact that the $B(M1)$ values for the regular and irregular bands of ^{196}Pb are similar also implies a similar degree of collectivity, as will be discussed below.

B. $M1$ transition rates

In the semiclassical model of Dönau and Frauendorf [27], the enhanced $B(M1)$ values in the dipole bands are due to structures involving deformation aligned high-K protons and rotation aligned high-j neutrons. In this strong-coupling scheme, the proton and neutron contributions to the magnetic moment reinforce each other, resulting in a large component of the magnetic moment perpendicular to the angular momentum. Various authors have made use of this geometrical picture to interpret the experimental $B(M1)/B(E2)$ ratios and $B(M1)$ values within the dipole bands. While calculations within the framework of this model have qualitatively reproduced the measured values (providing support for the high-K proton interpretation), detailed configuration assignments based on $B(M1)$ measurements have not been forthcoming.

One possible explanation for the difficulties encountered in the application of the Dönau and Frauendorf model to dipole bands in the Pb isotopes may be that the strong-coupling formalism used in this model is not valid at the small deformations encountered in these bands. The $M1$ properties of the oblate bands in Pb isotopes were recently studied using the tilted axis cranking (TAC) approach [27]. This model predicts that the $B(M1)$ values decrease with increasing spin since the tilting of the quasiparticle angular momentum toward the spin axis results in a reduction of the perpendicular component of the magnetic moment. However, when the results of TAC calculations for ^{198}Pb were compared to the experimentally measured $B(M1)$ values, the predicted decrease was not observed [27]. Clearly, in order to understand the underlying proton and neutron configurations in the dipole bands, both accurate lifetime measurements and refined theoretical calculations are necessary.

The experimentally determined $B(M1)$ values for bands 2 and 3 in ^{196}Pb are presented in Fig. 9. The magnitude of the $B(M1)$ values in each band are similar, with average values of ~ 1.5 W.u. These values are com-

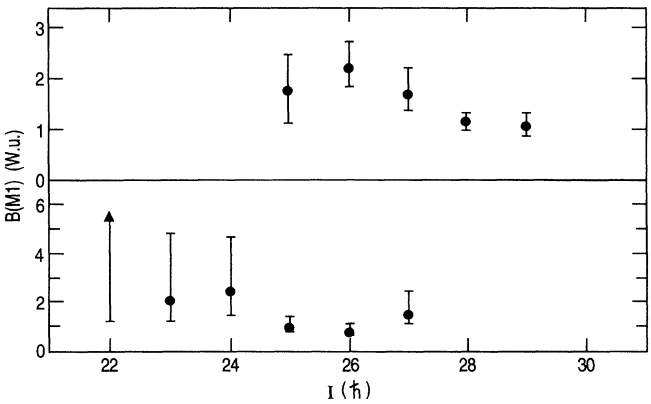

FIG. 9. Experimental $B(M1)$ values for band 3 (top), and band 2 (bottom). The data points presented for band 3 correspond to the assumption of spin $16\hbar$ at the bottom of the band.

parable to those obtained in other lifetime measurements in ^{197,198}Pb [16,9,17]. The spin dependence of the $B(M1)$ values evident in Fig. 9 is also consistent with previous measurements. One somewhat surprising result is that the $B(M1)$ values in the irregular band are comparable to those in the regular band.

1. Regular band

As discussed above, the $B(M1)$ values in the regular band (band 2) of ^{196}Pb exhibit some spin dependence. Since this band appears to be of rotational character, a comparison of the dependence of the $B(M1)$ and $\mathcal{J}^{(2)}$ values with rotational frequency is useful. Figures 10(a) and (b) shows that, despite large experimental errors, the $B(M1)$ values exhibit some correlation with $\mathcal{J}^{(2)}$. A similar correlation is present in band 3 of ^{198}Pb, as shown in Figs. 10(c) and (d). In each case, the maximum $B(M1)$ values are reached near peaks in the $\mathcal{J}^{(2)}$ curve. One might expect that as additional pairs of quasineutrons align, an increase in $B(M1)$ would result from the enhancement of the magnetic moment.

It should be pointed out that there is also a rather large increase in the $B(M1)$ values in band 1 of ^{198}Pb at $\hbar\omega \sim 0.45$ MeV, however, the $\mathcal{J}^{(2)}$ curve remains flat. Also, neither the $B(M1)$ nor the $\mathcal{J}^{(2)}$ values in the regular band of ^{197}Pb exhibit significant frequency dependence. These results point to the need for detailed calculations of quasiparticle alignments and interaction strengths in the crossing regions as well as high quality lifetime measurements for comparison.

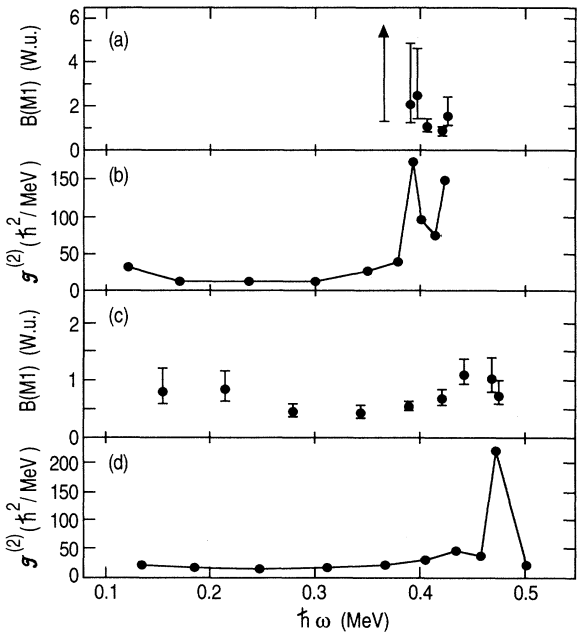

FIG. 10. Experimental $B(M1)$ (a) and dynamic moment of inertia $\mathcal{J}^{(2)}$ (b) values as a function of rotational frequency for band 2 in ^{196}Pb. Experimental $B(M1)$ (c) and $\mathcal{J}^{(2)}$ (d) values for band 3 in ^{198}Pb (in the notation of Ref. [10]). The experimental $B(M1)$ values in ^{198}Pb were derived from the measured lifetimes of Ref. [9] and the measured branching ratios of Ref. [17].

2. Irregular band

The measured $B(M1)$ values in the irregular band are comparable to those in the regular band of ^{196}Pb and to those in other regular dipole bands in the region. This result is in contrast to the case of ^{197}Pb, where the $B(M1)$ values within the irregular band were, on average, about a factor of 2 smaller than those in the regular bands. Due to the absence of $E2$ branches for comparison, it was not possible to establish the degree of quadrupole collectivity within the irregular structure of ^{196}Pb. However, from the lack of measurable $E2$ branches, one may infer that the degree of quadrupole deformation associated with this band is comparable to that of the regular bands.

Within the framework of the geometrical model, the presence of such large $B(M1)$ values in an apparently nonrotational structure would be somewhat unexpected. However, these results are consistent with the picture of a rotational structure undergoing quasiparticle alignment, as described above. It is worth pointing out that the RDM measurements in the irregular band of ^{197}Pb [17] cover the frequency region below the suggested BC crossing, in contrast to the current measurement where the lifetimes above the suggested BC crossing are accessible to DSAM measurements. Hughes *et al.* [16] report that the higher-lying transitions in the ^{197}Pb band exhibit no Doppler broadening in a DSAM measurement. However the presence of very low-energy transitions at the top of the band (in the region of the second backbend) could result in effective lifetimes longer than the stopping time of the residues in the backing. By comparison, in the case of ^{196}Pb the transition energies above the first backbend exhibit a regular increase with spin, resulting in lifetimes accessible to measurement by the DSAM. Thus, it is possible that in ^{197}Pb, an $M1$ enhancement may also exist at frequencies beyond the alignment of the $i_{13/2}$ neutrons.

Estimates of $B(M1)$ values based on the Dönau and Frauendorf model were presented in Ref. [17] for various proton configurations likely to play a role in the dipole bands. Depending on the number of $i_{13/2}$ neutrons involved, the $B(M1)$ estimates for the $\pi(h_{9/2}\otimes s_{1/2})$ configuration range from ~ 0.5 to ~ 2 Weisskopf units. While these simple estimates are consistent with the measured values, estimates based on other proton configurations yield similar results. However, independent of the adopted proton configuration, this model does give a qualitative interpretation of the increase in the $B(M1)$ values above the backbend. Following the alignment of $i_{13/2}$ quasineutrons, the magnetic moment of the system will be substantially enhanced due to the neutron contribution (see for example, Table V of Ref. [17]). Therefore, the interpretation of the irregular bands in terms of rotational structures based on configurations with some degree of signature splitting, which undergo quasineutron alignments seems plausible and consistent with experimental observations.

IV. SUMMARY

The level structure of ^{196}Pb has been measured and the lifetimes of states in two of the $\Delta I = 1$ bands (bands 2 and 3 in Fig. 2) have been determined in a DSAM measurement. A fourth dipole band (band 4) has been observed with regular transition energies. A comparison of the properties of this band with those of the other regular bands suggests a similar structure.

The $B(M1)$ values for states in both the irregular band and the strongest of the regular bands (band 2) have been extracted from the lifetime measurements. Both bands exhibit similar $M1$ strength, $B(M1)_{\rm avg} \sim 1.5$ W.u. It was shown that there may be a correlation between the $B(M1)$ and $\mathcal{J}^{(2)}$ values as a function of $\hbar\omega$ for the regular band. Similar characteristics were demonstrated for one of the dipole bands in ^{198}Pb [9,10]. The $B(M1)$ values within the irregular band in ^{196}Pb, on the other hand, were found to be much larger than those measured for a similar band in ^{197}Pb [17]. It is proposed that the contribution to the magnetic moment from the additional aligned quasineutrons above the strong backbend at $\hbar\omega = 0.25$ MeV is responsible for the large $B(M1)$ values in the irregular band of ^{196}Pb.

The TRS and cranking calculations of Refs. [6,10] suggest configurations based on $(h_{9/2} \otimes i_{13/2})$ or $h^2_{9/2}$ quasiprotons and $i_{13/2}$ quasineutrons for the regular bands. The large $B(M1)$ values are then attributed to the high-K quasiproton configurations coupled to rotation-aligned quasineutrons. The irregular bands are likely based on the $(h_{9/2} \otimes s_{1/2})$ quasiproton configuration. It is suggested that the apparent "irregularity" in these bands is in fact due to signature and alignment effects in rotational structures, and the regular bands are special cases of "shear" bands. Perhaps 3D cranking will give a more appropriate description of the dipole bands of this mass region. At present, the question of verification of configuration assignments based on $B(M1)$ measurements remains open.

This work was supported in part by the Department of Energy, Nuclear Physics Division under Contract Nos. DE-FG05-88ER40441, W-31-109-ENG-38, DE-AC07-76ID01570, DE-FG02-87ER4036, and by the National Science Foundation under Grant No. PHY88-02279.

[1] E. F. Moore *et al.*, Phys. Rev. Lett. **63**, 360 (1989).
[2] R. V. F. Janssens and T. L. Khoo, Annu. Rev. Part. Nucl. Sci. **41**, 321 (1991).
[3] A. J. M. Plompen *et al.*, Nucl. Phys. **A562**, 61 (1993).
[4] B. Fant *et al.*, J. Phys. G **17**, 319 (1991).
[5] M-G. Porquet *et al.*, J. Phys. G **20**, 765 (1994).
[6] J. R. Hughes *et al.*, Phys. Rev. C **47**, R1337 (1993).
[7] P. J. Dagnall *et al.*, J. Phys. G **19**, 465 (1993).
[8] F. Hannachi *et al.*, Proceedings of International Conference on Nuclear Structure at High Angular Momentum, Ottawa, Canada, 1992 (Report No. AECL-10613, Vol. 2, 1992).
[9] T. F. Wang *et al.*, Phys. Rev. Lett. **69**, 1737 (1992).
[10] R. M. Clark *et al.*, Nucl. Phys. **A562**, 121 (1993).
[11] R. M. Clark *et al.*, Phys. Lett. B **275**, 247 (1992).
[12] G. Baldsiefen *et al.*, Phys. Lett. B **275**, 252 (1992); G. Baldsiefen *et al.*, Nucl. Phys. **A574**, 521 (1994).
[13] A. Kuhnert *et al.*, Phys. Rev. C **46**, 133 (1992).
[14] R. M. Clark *et al.*, Z. Phys. A **342**, 371 (1992).
[15] G. Baldsiefen, H. Hübel, F. Azaiez, C. Bourgeois, D. Hojman, A. Korichi, N. Perrin, and H. Sergolle, Z. Phys. A **343**, 245 (1992).
[16] J. R. Hughes *et al.*, Phys. Rev. C **48**, R2135 (1993).
[17] R. M. Clark *et al.*, Phys. Rev. C **50**, 84 (1994).
[18] E. F. Moore *et al.*, Phys. Rev. C **48**, 2261 (1993).
[19] Physics Division Annual Review, Argonne National Laboratory, Report No. ANL–93/12 34, 1993.
[20] H. Emling *et al.*, Phys. Lett. B **217**, 33 (1989); H. Emling *et al.*, in Proceedings of the Twenty-Second School on Physics, Zakopane, Poland, 1987, edited by R. Broda and Z. Stachura, Instytut Fizyki Jądrowej w Krakowie Report No. IFJ 1956/PL, p. 151.
[21] J. F. Ziegler, J. P. Biersack, and U. Littmark, *The Stopping and Range of Ions in Solids* (Pergamon, New York, 1985).
[22] H. Emling *et al.*, Nucl. Phys. **A419**, 187 (1984).
[23] R. Bengtsson and W. Nazarewicz, Z. Phys A **344**, 269 (1989).
[24] J. J. Van Ruyven *et al.*, Nucl. Phys. **A449**, 579 (1986).
[25] J. Penninga, W. H. A. Hesselink, A. Balanda, A. Stolk, H. Verheul, J. Van Klinken, H. J. Riczibos, and M. J. A. De Voigt, Nucl. Phys. **A471**, 535 (1987).
[26] S. Frauendorf, Nucl. Phys. **A557**, 259c (1993).
[27] F. Dönau and S. Frauendorf, in *Proceedings of the Conference on High Angular Momentum Properties of Nuclei*, Oak Ridge, 1982, edited by N. R. Johnson (Harwood Academic, New York, 1982), p. 143.